Wind and Structures, *Vol. 23, No. 1 (2016) 000-000*
DOI: http://dx.doi.org/10.12989/was.2016.23.1.000

Numerical and experimental study of unsteady wind loads on panels of a radar aerial

Ana Scarabino*[1], Mariano García Sainz[2,3], Federico Bacchi[1], J. Sebastián Delnero[2.3] and Andrés Cánchero[2]

[1]*Grupo de Fluidodinámica Computacional, Universidad Nacional de La Plata, Calle 116 e/47 y 48, 1900 La Plata, Argentina*
[2]*Laboratorio de Capa Límite y Fluidodinámica Ambiental, Universidad Nacional de La Plata, Calle 116 e/47 y 48, 1900 La Plata, Argentina*
[3]*Consejo Nacional de Investigaciones Científicas y Técnicas, Avda. Rivadavia 1917, CP C1033AAJ, Cdad. de Buenos Aires, Argentina*

(Received July 4, 2015, Revised May 2, 2016, Accepted May 15, 2016)

Abstract. This work experimentally and numerically analyzes the flow configurations and the dynamic wind loads on panels of rectangular L/h 5:1 cross section mounted on a structural frame of rectangular bars of L/h 0.5:1, corresponding to a radar structure. The fluid dynamic interaction between panels and frame wakes imposes dynamic loads on the panels, with particular frequencies and Strouhal numbers, different from those of isolated elements. The numerical scheme is validated by comparison with mean forces and velocity spectra of a panel wake obtained by wind tunnel tests. The flow configuration is analyzed through images of the numerical simulations. For a large number of panels, as in the radar array, their wakes couple in either phase or counter-phase configurations, changing the resultant forces on each panel. Instantaneous normal and tangential force coefficients are reported; their spectra show two distinct peaks, caused by the interaction of the wakes. Finally, a scaled model of a rectangular structure comprised of panels and frame elements is tested in the boundary layer wind tunnel in order to determine the influence of the velocity variation with height and the three-dimensionality of the bulk flow around the structure. Results show that the unsteady aerodynamic loads, being strongly influenced by the vortex shedding of the supporting elements and by the global 3-D geometry of the array, differ considerably on a panel in this array from loads acting on an isolated panel, not only in magnitude, but also in frequency.

Keywords: wake interaction; dynamic loads; Strouhal number

1. Introduction

It is a known fact that a 2D bluff body immersed in a flow stream introduces in the flow periodic vortex shedding, which causes fluctuating loads that in turn can produce mechanical vibrations. Other mechanisms which cause fluctuating loads are turbulent buffeting, aeroelastic instability and acoustic resonance (Fitzpatrick *et al*. 1988). Several experimental and numerical studies have been carried out to obtain detailed information about the structure of such flows and

*Corresponding author, Professor, E-mail: scarabino@ing.unlp.edu.ar

http://www.techno-press.org/?journal=was&subpage=8 ISSN: 1226-6116 (Print), 1598-6225 (Online)

the different mechanisms of fluid-structure interaction (So *et al*. 2001, Blackburn and Henderson 1999, Freitas 1995). In those cases involving an array of cylinders, the flow is naturally more complex than around a single cylinder configuration. Lam *et al.* (2003) demonstrated that the flow around four cylinders in a square array shows particular vortical structures, which are not seen in a 2-cylinder configuration. The force coefficients and Strouhal numbers are modified by the non-linear interaction with other bodies, being influenced by their distance, diameter, orientation and number of elements. Due to its significance in multiple engineering problems, this interaction has been and is studied in a large number of particular cases. Sumner *et al*. (2000) studied fluid-structure interaction and its effects on the flow configuration, bistable flows and Strouhal number variations. More recently, the flow field around a 5:1 rectangle was analyzed using Detached Eddy Simulation by Mannini *et al*. (2009), and different interaction mechanisms between two rectangular cylinders were numerically studied by Chatterjee *et al.* (2010). It is clear from these and other studies, that the frequencies and intensities of aerodynamic loads strongly depend on the array geometry, so each problem requires a specific study in order to determine the particular fluid dynamic loads and their spectral characteristics.

All the mentioned works study wake interaction of bodies with the same geometries and dimensions (cylinders, rectangles, etc.). In the present case, the physical problem is the determination of wind loads on radar panels with a rectangular section of approximately 5:1 aspect ratio, at an angle of incidence of 10^{o}, mounted on a structural frame of smaller 0.5:1 structural elements. This configuration or similar ones are also typical of wind breaks and anti-jet barriers, solar panels, wind and shadow screens, solar dryers, etc., where the flow experiences the interaction of bodies of different geometries and dimensions. The results are presented as a case study, which shows the strong influence of the supporting structure on the dynamic loads on panels.

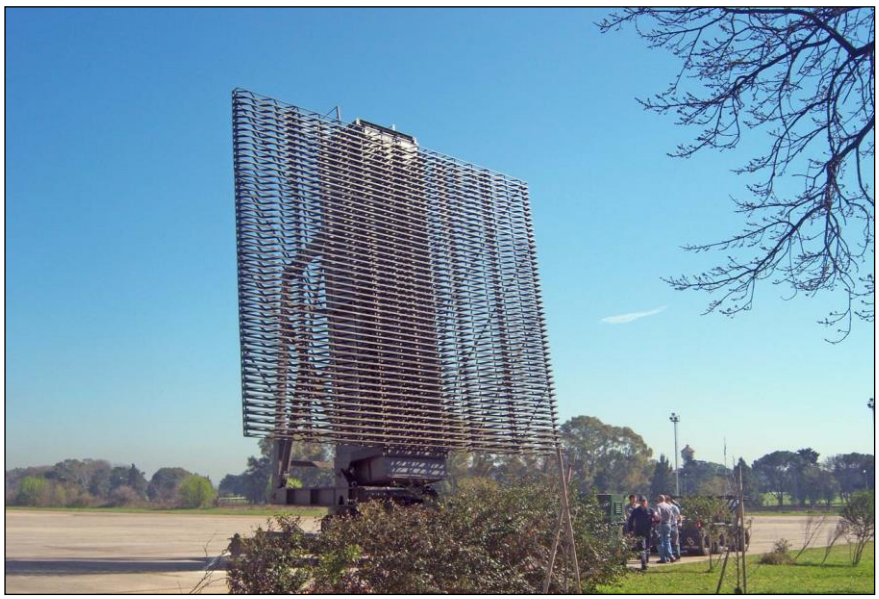

Fig. 1 Radar aerial similar to the one studied

Fig. 1 shows a radar structure similar to the one studied in this paper. The goal is to determine the unsteady aerodynamic loads on each panel and to understand their causes. In order to do so, a full scale two-dimensional array of three panels and four structural bars was numerically and experimentally analyzed. The numerical model was then employed for a two-dimensional study of a structure of ten panels with their corresponding structure. Finally, with the purpose of analyzing the influence of the three-dimensional effects, experimental tests were carried out using a 1:23 model in an atmospheric boundary layer flow. Results show the interaction of vortex shedding from the different elements and its influence on the unsteady aerodynamic forces on the panels. The 3-D model allowed to measure the local increments of aerodynamic loads due to the wind variation with height, the interference of the central column and the three-dimensional flow around the bulk structure. Additionally, global normal and tangential loads on the whole structure were measured and force coefficients are reported for different wind directions.

2. Methodology

2.1 Wind tunnel testing of a 2D full scale model

2.1.1 Full scale 2-D wind tunnel experiments

A physical model was built with three 0.225 m chord by 0.044 m height section and 0.8 m span wood panels. In addition, structural elements of 0.04 m by 0.02 m were placed at the locations shown in Fig. 2. "Tangential" and "normal" directions in reference to the panel are shown in the figure. "Horizontal" always refers to the wind direction and "vertical" to its normal.

For this wind tunnel experiment, lateral plates helped to keep the mean flow two-dimensional. Measurements were carried out in a range of velocities between 5 and 17 m/s in order to verify the flow´s and load coefficients´ independence from the Reynolds number. The mean flow velocity was acquired using a Dantec Flowmaster anemometer located 1.5 m upstream of the array. A 2-component strain gage balance with Vishay 2310 signal amplifiers was used for measurements of the aerodynamic loads acting on the central rectangular element. The balance was placed at one end and a "dummy" balance with no strain gages was placed at the other end. Symmetry of loads was verified and then the strain gage balance was calibrated in the experiment setup in order to measure the total load. The instantaneous longitudinal and vertical velocity components in the wake, were measured with a Dantec Streamline CTA 90C10 hot wire anemometer, with X probes 51R51, at downstream distances of h and $2h$, with h being the panel height. Signals were acquired at 2000 Hz per channel and low-pass filtered at 1000 Hz. These frequencies were chosen in order to adequately capture the velocity fluctuations due to vortex shedding. Vortex shedding frequencies were identified from the vertical velocity spectral peaks in the wake, both in the wind tunnel measurements and in the numerical simulations, following a methodology previously employed in similar experiments (Scarabino *et al*. 2005). In order to determine the Strouhal number, instantaneous velocity data were acquired across the shear layer in the wake of the section, as sketched in Fig. 2, and the vortex shedding frequency was deduced from the marked spectral peaks of the velocity fluctuations.

Fig. 3 shows the experimental array in the wind tunnel test section, and Table 1 summarizes the employed instrumentation.

The analysis considered the operating position of the radar aerial, which is 10^o with respect to the vertical, giving the radar panels an incidence of 10^o with respect to the horizontal wind direction.

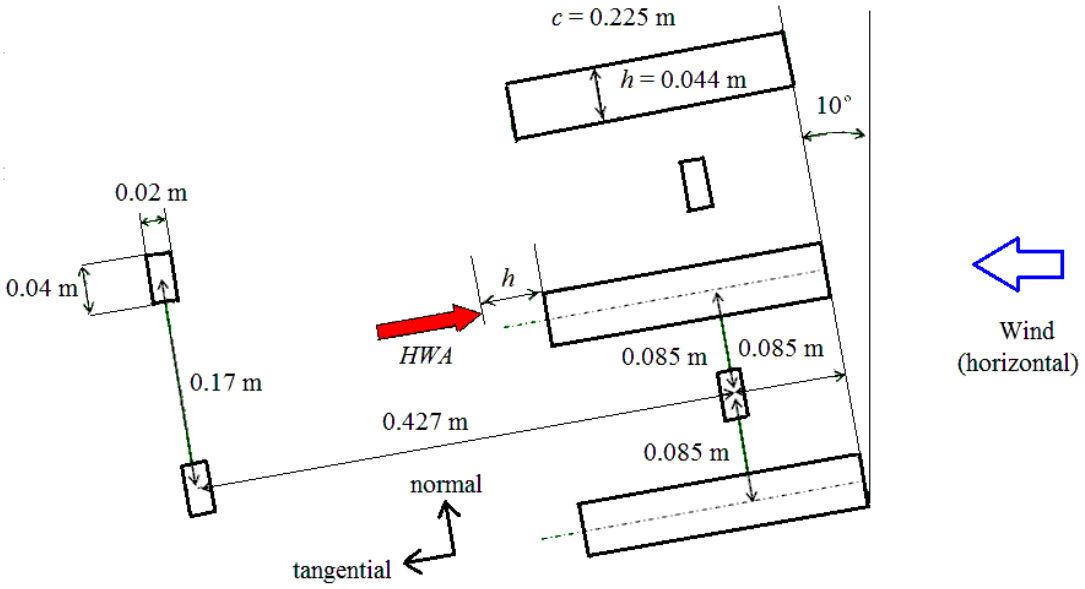

Fig. 2 Full scale panel array for numerical and experimental analysis at an incidence of 10°. "*HWA*" shows the position of the hot wire anemometer probe at a distance h = 0.044 m from the central panel

Fig. 3 Radar panels (wood), structure bars (blue) and vertical support of hot wire anemometer probe. View from downstream

Table 1 Wind tunnel experiments: instrumentation details

2-D panel full scale	-	DANTEC FlowMaster 54N60	Mean flow velocity reference
	-	DANTEC StreamLine CTA 90C10	Instantaneous two component velocity measurements
	-	55R51 X-type probes	
	-	2-component strain gauge balance	Aerodynamics loads
	-	Vishay 2310 signal amplifier	

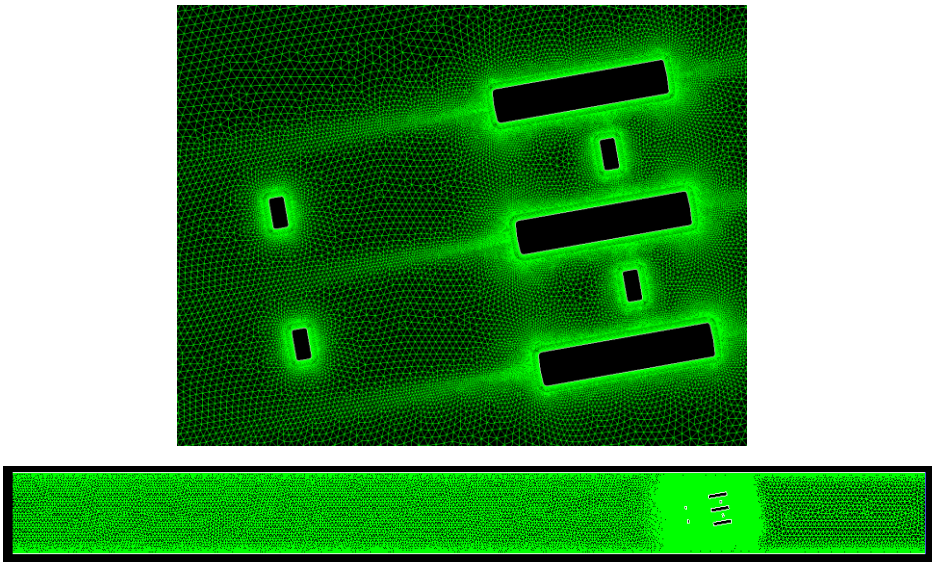

Fig. 4 2-D mesh for numerical simulation of wind tunnel tests

2.1.2 Numerical simulation of full scale 2-D wind tunnel arrangement

A 2-D numerical simulation was carried out in a Quadcore PC at 2.66 GHz with the commercial software package Fluent 6.3, with a mesh of approximately 180000 triangular elements and boundary layer refinements, adequate for the turbulence model *k-ω SST* (details of the mesh shown in Fig. 4). Hardware limitations led to the choice of a 2-D simulation with a *RANS* (Reynolds-Averaged Navier-Stokes) turbulence model, therefore the numerical results are restricted to this condition. The *k-ω SST* model was selected, first because its proved ability for modeling detached flows with periodic vortex shedding, (Catalano and Amato, 2003), and second because of previous satisfactory experiences with this model for these types of flows (Bacchi *et al*. 2007). The solver was second-order implicit in time and space for momentum and for the turbulent parameters k and ω, with a time step of 5e-5 s. The local CFL number was for all cells between 0 and 20, and its mass-averaged value for the whole domain was 0.12. The boundary layer meshes were successively refined until meeting the criterion of $y+ < 5$, adequate to properly model the boundary layer with the chosen turbulence model (Menter 1994). The variation in the computed aerodynamic loads was negligible for the last refinements, which was considered an acceptable criterion for ensuring mesh

independence. The domain was extended up to 8 panel chords (*c*) upstream and 30 *c* downstream, and 20 panel heights (*h*) in the vertical direction, which corresponds to the wind tunnel height. Larger distances for the inlet and outlet boundaries did not change the results, so the domain size was considered adequate for the simulation.

Boundary conditions included a constant velocity inlet, constant pressure outlet, and no slip condition at the walls.

The purpose of this simulation was to numerically reproduce the wind tunnel experiments, in order to get a deeper insight of the flow structure and to validate the numerical model, which was later used for modeling the flow around an array of ten panels and their supporting structure. A first case was run with one isolated panel at 0^o of incidence, in order to compute its vortex shedding frequency and Strouhal number without the influence of surrounding panels and frame. Then, an array of three panels and four structural elements was modeled, reproducing the experiments detailed in section 2.1.1. Once the numerical results for the global flow pattern and the wake were stabilized in a periodic configuration, the field variables were studied in order to understand the flow structure and the unsteady loads on the rectangular panels. This study focuses on the central panel, as representative for this configuration, which frequently involves a large number of elements.

2.2 2D numerical simulation of 10 panels in free flow

A 2D simulation was carried out for a section composed of 10 panels and their corresponding frame elements. The domain extension was of approximately 70 *c* or 7 array heights upstream, 150 *c* or 15 array heights downstream and 15 array heights in vertical direction. Boundary conditions for this case included free stream velocity upstream and at the domain top and bottom, and constant pressure at the downstream boundary. This array allowed multiple possibilities of fluid-dynamic interaction, which were investigated. The analysis focused on the velocity field evolution and the unsteady wind loads on the panels. The model parameters were a hybrid mesh of approximately 4e5 elements, with adequate discretization of the boundary layer and the wake regions (Fig. 5), incompressible unsteady flow, second-order implicit solver for space and time and turbulence model *k-ω SST*.

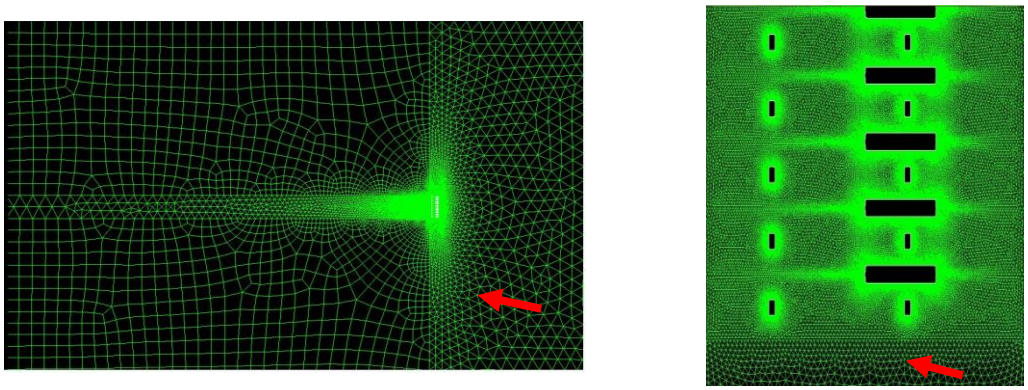

(a) Whole computational domain (b) Detail of the array

Fig. 5 Mesh around the 10-panel array. The arrow indicates the wind direction (10^o)

2.3 Wind tunnel testing of a 3-D model

In order to consider three-dimensional effects, a 1:23 scale model of an 8 m x 7 m structure with 20 panels, was built and tested in the boundary layer wind tunnel at the Boundary Layer and Environmental Fluid Dynamic Laboratory, at the University of La Plata (Fig. 6). The test section is 1.4 m wide and 1 m high.

Seven panels at different heights were instrumented with pressure taps: 4 on each front and 3 on each rear face (Fig. 7). Pressures at the 49 taps, were measured using a Pressure Systems multimanometer, model NetScanner 98RK-9816. Five hundred instantaneous values per channel were acquired at a sampling rate of 4 Hz per channel and averaged to get the mean value at each point. Even if instantaneous pressures were sampled, only mean pressures were considered. According to Bergh and Tidgeman's model (Bergh and Tidgeman 1965) the measuring system dynamical response has negligible effects on the mean values for this tests. The atmospheric turbulent boundary layer was modeled by means of roughness elements and adjustable vanes located at the test section entrance (Fig. 8). The mean velocity was measured with a Dantec Flowmaster hot wire anemometer.

Finally, horizontal normal and tangential forces on the whole model structure were measured with a two-channel aerodynamic balance fixed to the supporting column. The complete test assembly includes the aerodynamic balance (2-axis balance provided with a set of strain gauges), which is connected through a cable to the National Instruments amplified acquisition system. The cable is connected through the front-mounting terminal block (NI SXCI 1314) for the (NI SXCI 1520) universal strain gauge input module. The NI SCXI 1000 chassis is connected through a USB cable to the PC. A LabView Virtual Instrument was created in order to read, acquire and convert (voltage to load) data from the balance. Table 2 synthesizes the instrumental.

Fig. 8 shows the boundary layer velocity profile, fitted with a 0.21 exponent power law, corresponding to open suburban or rural environment with obstacles such as trees or low buildings (Sachs 1978), and the corresponding turbulence intensity profile.

Table 2 Wind tunnel experiments, instrumentation for the 3-D model

	DANTEC FlowMaster 54N60	Mean flow velocity reference
	Pressure Systems NetScanner 98RK-9816	Pressure measurements
3-D model scale 1:23	2-component strain gage balance National Instruments NI SCXI 1000 (chasis) NI SCXI 1600 (digitalizer) NI SCXI 1520 (universal strain gauge input) NI SCXI 1314 (terminal block)	Aerodynamics loads

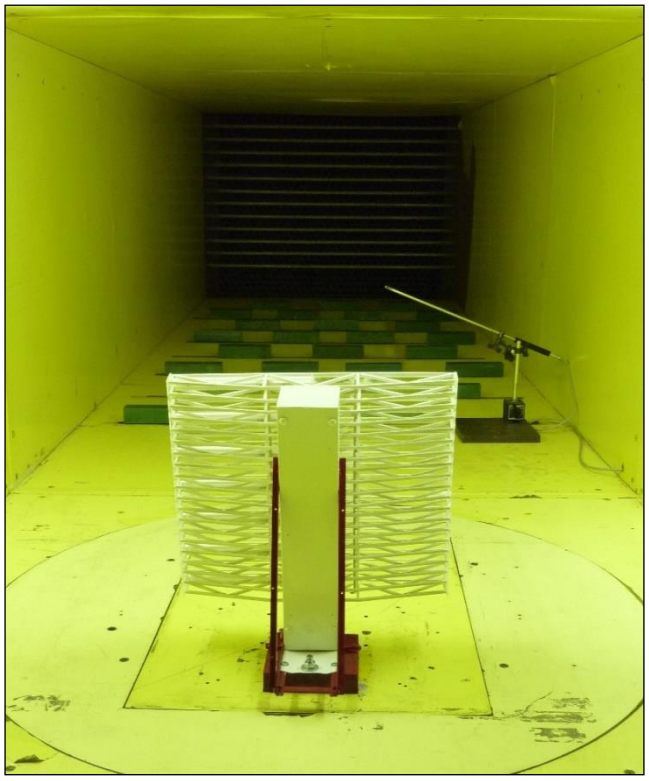

Fig. 6 Radar model in the boundary layer wind tunnel

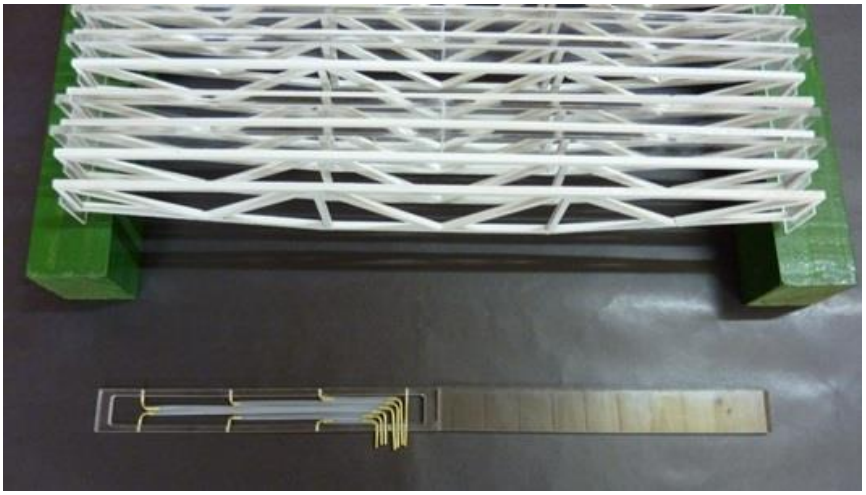

Fig. 7 Close view to the radar model and a panel with pressure taps. These are located on the front and rear of each panel

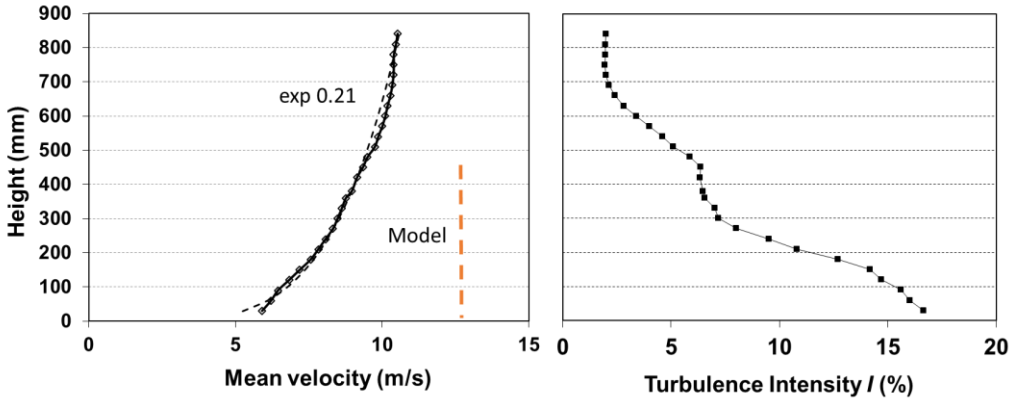

Fig. 8 Boundary layer velocity, power law fit (dashed) and turbulence intensity profiles

Fig. 9 shows the normalized turbulence spectrum at the model height. As shown, the spectrum was in good agreement with the Von Karman-Harris' analytical approximation (Holmes 2001).

$$\frac{fS_u}{\sigma_u^2} = \frac{4(fL_u/U)}{\left[1+70.8(fL_u/U)^2\right]^{5/6}} \tag{1}$$

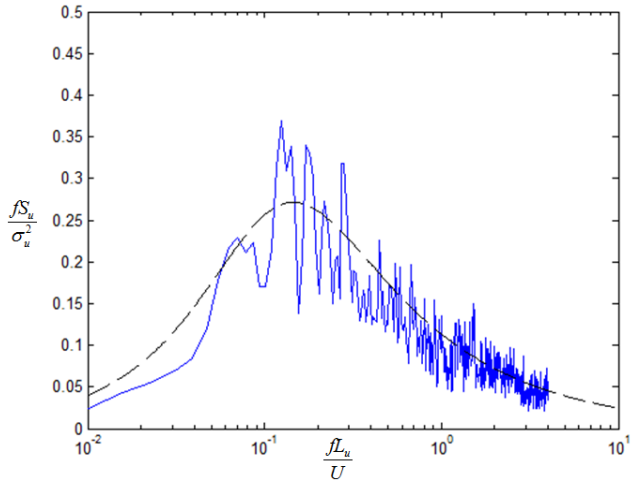

Fig. 9 Normalized spectrum of longitudinal velocity fluctuations (continuous) – Von Karman-Harris spectrum (dashed). U = 9.5 m/s

The integral time scale T_u for the velocity fluctuations was approximated with the time lag $\tau_{1/e}$, for the 1/*e* value of the autocorrelation function (Kaimal and Finnigan 1994). The integral length scale for the longitudinal fluctuations, L_u, was estimated from the integral time scale using "frozen flow theory", as $L_u = UT_u$, giving values close to 0.15 m.

3. Results

3.1 Full scale panels and frame in the wind tunnel: numerical and experimental results.

3.1.1 Flow field: numerical results

The flow field was primarily studied through numerical computations. Instantaneous velocity plots showed that the panel wake was strongly modulated by the vortex shedding of the upper and lower structural bars. The vortices shed by these two elements tended to lock in one of two possible configurations: either "in-phase", when vortices of the same sign (either clockwise or counterclockwise) were shed simultaneously from the bars above and below the radar panel, or "in counter-phase", when vortices of opposite rotation were shed at the same times. Fig. 10 shows both configurations, one at 0^o of incidence, and one at the operating angle of 10^o. In the counter-phase case at zero incidence, the structural elements caused a symmetric flow pattern on the panels, considerably reducing the fluctuating forces on it. These vortices, in either configuration, locally imposed their own shedding frequencies, and caused the increase and decrease of the static pressure along the panels upper and lower faces, with the consequent boundary layer periodic detachment and reattachment. Fig. 11 shows the instantaneous pressure distribution for the central panel surface at an incidence of 10^o, corresponding to the velocity field of Figure 10b. Reattachment zones can be seen to correspond to positive Cps. The vortices shed from the structure bars interacted and merged with the detached flow on the large panels, configuring a wake where all vortex systems coupled.

The pressure coefficient C_p is defined in the usual way as

$$C_p = \frac{P - P_\infty}{0.5\rho V^2} \tag{2}$$

P is static pressure, ρ the air density and V the free stream velocity. The reference pressure P_∞ is that of the free stream at the domain inlet boundary.

3.1.2 Velocity fluctuations spectra: numerical and experimental results

Fig. 12 shows the vertical velocity component (*v*) spectra, from both hot wire anemometer measurements and numerical computations, at downstream distances of one and two panel heights (*h*) from the central panel, in its wake (see Fig. 2), for the flow at 10^o of incidence. The first spectral peak was found at 60 Hz in the experiments and at 70 Hz in the numerical simulations, corresponding to Strouhal numbers based on the height of the rectangular structural element, of 0.218 and 0.254, respectively. These values are higher than those reported for isolated rectangular elements (Okajima 1982), but the discrepancies can be explained considering the interference effect of the different elements, which do not allow the shed vortices to grow up to the size they would reach if the obstacle were isolated in the flow, thus reducing the final vortices size and time scale and increasing their shedding frequency. Experiments showed a second spectral peak at 120 Hz, which

decays at a distance of *2h*. This peak was found with lower intensity in the numerical simulations. We speculate that this peak could be an effect of the wakes interaction.

The comparison between the vertical velocity fluctuation spectra of experimental and computational results shows a difference in *S(f)* intensity of one order of magnitude. The rms value of the velocity fluctuations was 4.73 m/s for the measurements and 10.98 m/s for the numerical simulation. Since the spectrum integrals must give the square of these values, this is consistent with the difference in *S(f)* intensities. We speculate that an explanation can lie in the fact that *RANS* methods filter the high frequency velocity fluctuations, which are dissipative, and increase the energy of the resolved (low frequency) eddies, so that the computed eddies are more energetic than those actually shed by the obstacles. But, as stated, this is speculation and deserves further investigation. Nevertheless, the spectral peaks were found at similar frequencies, which reinforces our confidence in the numerical results. The decay at high frequencies was steeper for numerical computations. This is caused by the *RANS* turbulence model, which, as mentioned, "filters" turbulence fluctuations of high frequencies.

Additionally, a simulation of a single rectangular panel at 0^o was run in order to determine its Strouhal number without interaction with the structural elements. With a free stream velocity of 11 m/s, the vortex shedding frequency was 40 Hz, giving a Strouhal number of 0.16, based on the element height. This Strouhal number is higher than other reported values for rectangular sections of similar aspect ratios. We speculate that a possible reason is the rounded edges ($R/h = 0.1$, being R the curvature radius). It has been shown (Vikram *et al.* 2012) that this feature increases the Strouhal number for square cylinders.

3.1.3 Force coefficients: numerical and experimental results

In all cases, reported coefficients are of tangential (t) and normal (n) forces, in the rectangular element frame of reference, instead of lift and drag coefficients in the wind frame of reference. The reason for this choice was the simplicity for structural computations when loads are referred to the structure principal axis.

The experimental facilities only allowed to measure mean forces. The non-dimensional force coefficients were computed and compared at different wind velocities between 5 m/s and 17 m/s in order to verify independence of Reynolds number, which was achieved. Table 3 details the force coefficients that were measured (only mean values at 10^o) and computed numerically. Differences between numerical and experimental mean values of force coefficients were under 10%.

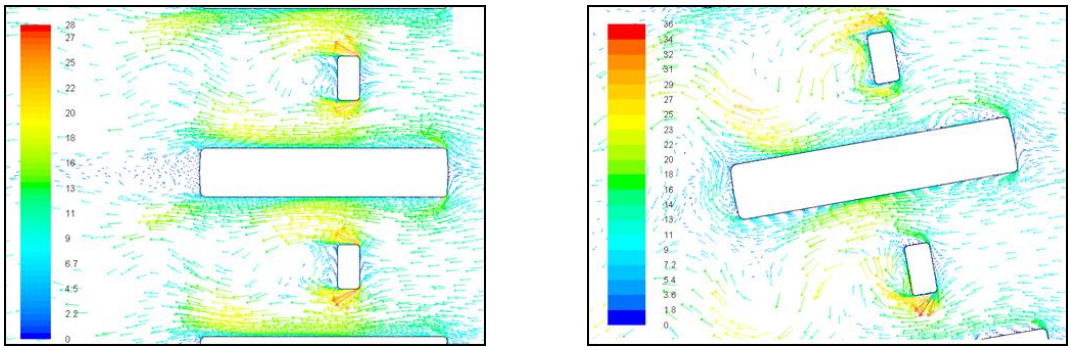

(a) 0^o Incidence – Vortex shedding in phase (b) 10^o Incidence – Vortex shedding in counter-phase

Fig. 10 Instantaneous velocity plots. Color map indicates velocity magnitude in m/s

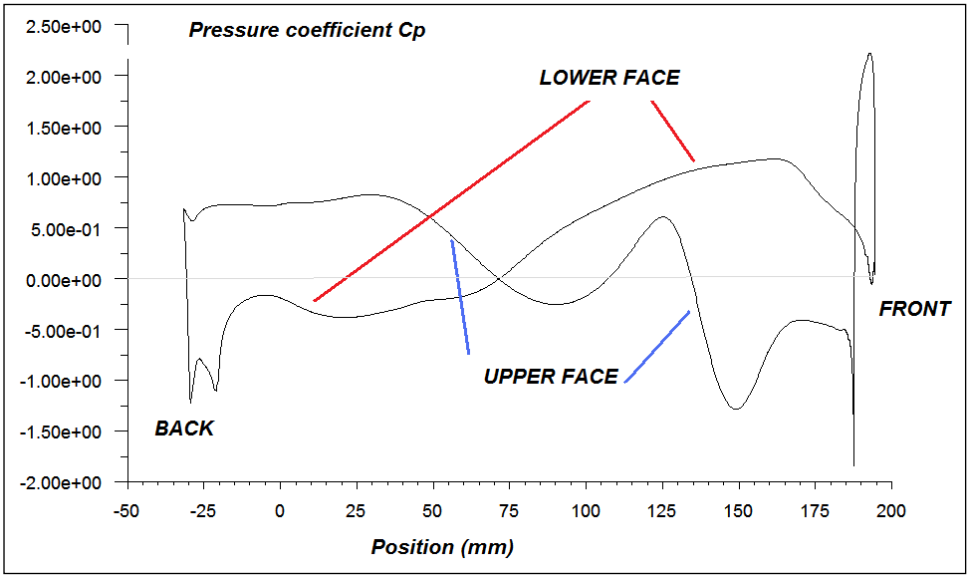

Fig. 11 Instantaneous pressure distribution on a panel surface with the array at 10°, modulated by the vortex shedding of structural elements

Table 3 Tangential (t) and normal (n) force coefficients on the central panel

NUMERICAL (v = 11 m/s), 10°				EXPERIMENTAL		DIF % Ct	DIF% Cn
Ct		Cn		Ct	Cn		
MEAN	0.427	MEAN	0.281	0.39	0.306	9.34	9.07
MAX.	0.74	MAX.	1.476				
MIN.	0.161	MIN.	-0.789				
RMS.	0.086	RMS.	0.448				

It is worth pointing out, as a relevant result for structural design, that the instantaneous normal force coefficient reached a maximum value of 1.47, five times its mean value.

3.1.4 Force spectra: numerical results

Instantaneous aerodynamic forces were not measured at the radar panels, but only computed numerically. Integration of pressure and shear stress gives the instantaneous normal and tangential forces on the panels. These fluctuating loads are induced mainly by the periodic vortex shedding of the structural frame elements and secondly by the panel wakes and their dynamic coupling with those of the frame. These time-varying normal and tangential forces were then processed in order to obtain their spectral distributions. These are shown in Fig. 13, for incidences 0° and 10° and V = 11 m/s. Fig. 13 also illustrates the origin of the spectral peaks at 10°.

The main normal and tangential loads frequency on the large central panel is 70 Hz, the same detected as the first peak in the wake velocity fluctuations. The second peak in the velocity fluctuations, found at 120 Hz, primarily affects the tangential loads - Figs. 10(a) and 10(b) -. The lower frequency loads around 40 Hz match the vortex shedding frequency of an isolated panel at 0^o, and could thus be an attenuated effect of the panel local influence in the flow field. This frequency of 40 Hz appears with secondary intensity in the loads spectra at 10^o and it is suppressed in the counter-phase configuration of the array at 0^o.

At 0^o the peak at 70 Hz prevails, although the overall load amplitude is lower. The second peak at 120 Hz contributes with smaller intensity, as seen in Figs. 13(a) and 13(b). Normal force fluctuations on the panel at 10^o (Fig. 13(d)) are of much larger amplitude than those at 0^o and the fluctuating tangential forces at both angles of incidence.

Mean force coefficients and velocity spectra obtained from the numerical and experimental results show an acceptable level of concordance, thus validating the numerical model for further simulations.

3.2 Multiple panels and frame in free flow (numerical simulation).

After validation with the experimental results of section 3.1, the numerical model was applied to an array of 10 panels with their supporting frame.

Turbulence intensity (I) contours were computed from the definition of the kinetic energy k for the k-ω turbulence model, and the local average velocity u_{avg} (Menter 1994)

$$k = \frac{3}{2}(u_{avg} I)^2 \tag{2}$$

It was found that when the number of panels increases, both types of vortex coupling, in phase and in counter-phase, from the structural bars, appear simultaneously on different panels. An analysis of Fig. 14 shows, for example, that the vortices shed above and below the third panel (from above) are coupled in counter-phase, generating a quasi-symmetrical wake, while at the fourth one the coupling is in phase, which increases the net force peaks on this panel, up to the levels computed in the previous section. The computation of the resultant forces on each individual panel gave results that did not differ significantly from those reported in section 3.13 for the limited array of three panels.

3.3 Load factor distribution (experimental)

With the goal of studying the three-dimensional effects that were ignored in the previous experiments and simulations, pressure measurements were carried out on selected panels of the 1:23 scale model of the whole radar structure shown in Fig. 6. Twenty-eight pressure tap pairs in the front and rear faces of some panels were uniformly distributed on selected panels. Increment load factors were computed and interpolated over the radar frontal area from the pressure difference between the front and rear faces as

$$f_i = \frac{\Delta P}{\Delta P_{ref}} \tag{3}$$

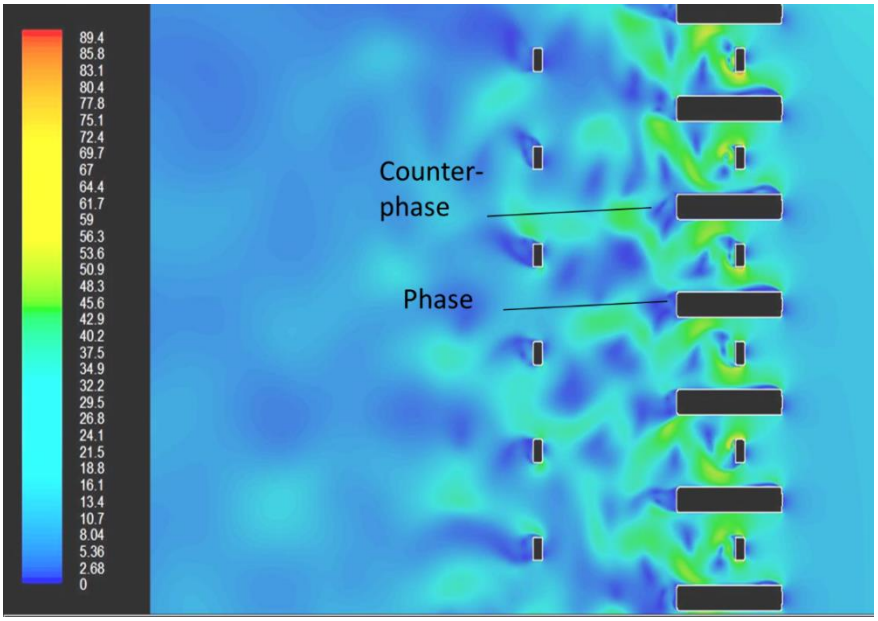

Fig. 14 Instantaneous turbulence intensity distribution. Forces on radar panels are modulated by the vortex shedding of structural bars, either in phase (worst condition) or in counter-phase

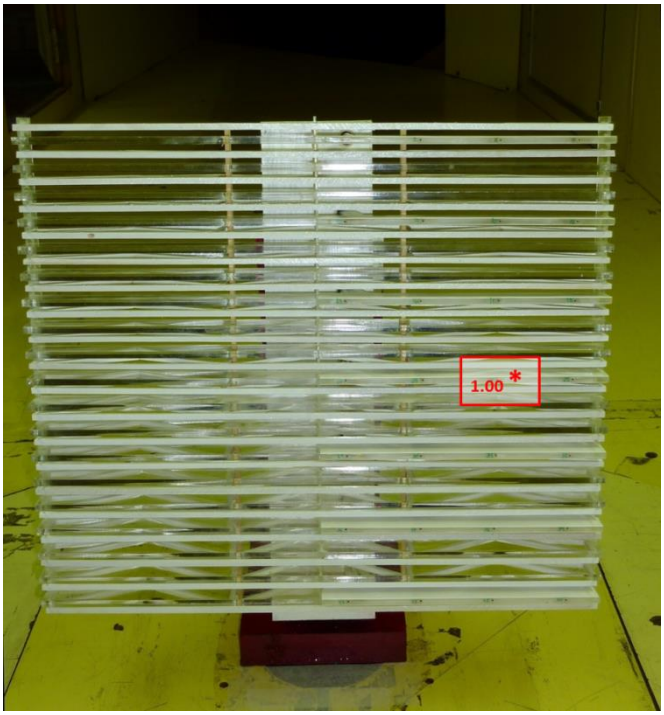

Fig. 15 Frontal view of radar model and reference point for incremental factors

ΔP_{ref} is measured on a central panel at the point indicated in Fig. 15, chosen because of its location as the most representative of the 2-D measurements and computations. The vertical plane parallel to the wind direction passing through this point was considered the closest to the 2-D simulation described in section 3.2. The aerodynamic force coefficients reported in Table 3 should be multiplied for each panel by factor f_i (distribution shown in Fig. 16 for different lateral wind incidences), which takes into account the wind variation with height, the interference with the supporting column and the three-dimensionality of the structure bulk flow.
For a lateral incidence of 15°, the loads on the outer panels facing the wind can increase by up to 95 % due to three-dimensional effects.

It is clear that these increments depend largely on the whole radar aspect ratio, the wind velocity direction and profile, and the geometry and extent of the rear supporting structure. They highlight the limitations of the two-dimensional analysis, and give orientations to safety coefficients to be used for the structural design of the aerial panels and joints.

3.4 Global 3-D force coefficients (experimental)

Although the motivation for this study was to obtain design loads for the radar panels, having built the model allowed obtaining global wind forces on the structure with little additional effort.

The dimensionless aerodynamic coefficients of the normal and lateral forces of the whole structure were obtained with the following formulas

$$C_{normal} = \frac{F_{normal}}{0.5\, S_{ref}\, \rho V_{ref}^{\,2}}$$

$$C_{lateral} = \frac{F_{lateral}}{0.5\, S_{ref}\, \rho V_{ref}^{\,2}} \qquad (4)$$

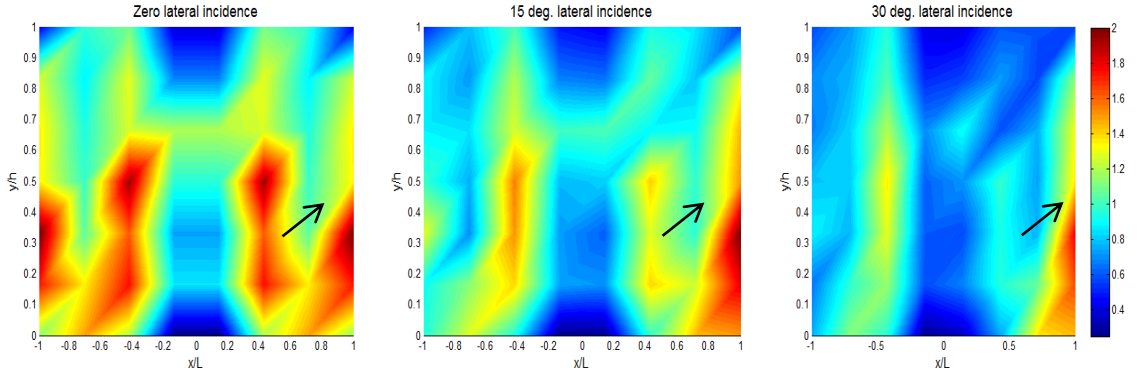

(a) Lateral incidence 0° (b) Lateral incidence 15° (right side toward wind) (c) Lateral incidence 30° (right side toward wind)

Fig. 16 Distribution of incremental factors *fi* for local wind forces on panels, for different lateral incidence. The black arrow indicates the reference point

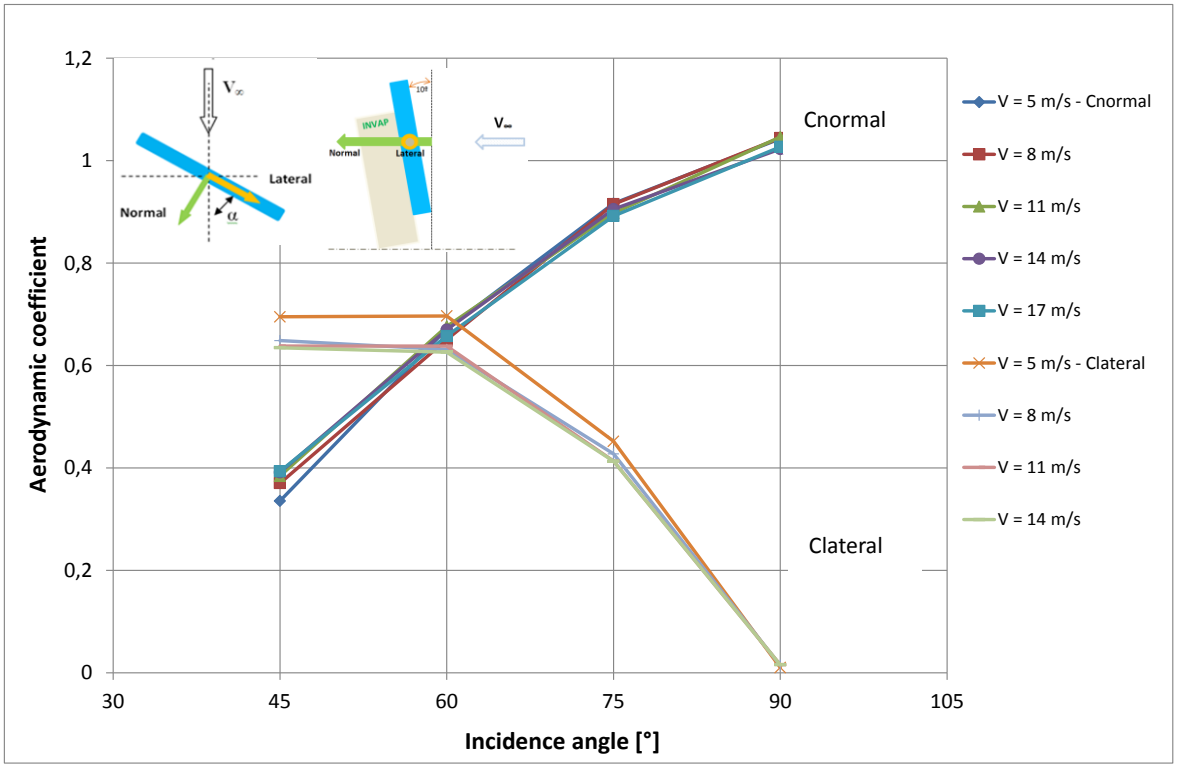

Fig. 17 lateral and normal coefficients for the whole radar aerial

where S_{ref} is the radar area, V_{ref} is the reference velocity measured at the structure height in the upstream boundary layer flow, and ρ is the air density in the wind tunnel corrected for temperature. It must be pointed out that the radar plane has an inclination of 10^o with respect to the vertical axis, and the measured forces are in a horizontal plane, so what we call the "normal" force is actually its projection on the horizontal plane, 1.5% less than real normal values, since $\cos(10^o) = 0.985$. Lateral forces are not affected by the radar vertical inclination (see sketch in Fig. 17).

The structure was rotated around a vertical axis in order to compute normal and lateral coefficients for different lateral incidence angles of the wind. Fig. 17 shows the normal and lateral coefficients for different incidence angles and wind velocities. As shown, the results were independent of the Reynolds number in the tested range. The normal coefficient for a square flat plate perpendicular to the wind is 1.18 (Hoerner 1957). For this open but complex structure its average value was 1.04.

4. Conclusions

The results of these numerical and experimental studies show that the fluid-dynamic coupling of wakes in an array of different elements at 0^o and 10^o of incidence noticeably modifies the vortex

shedding configuration, and with it, the spectra of periodic loads on slender structures: The imposed local frequencies and instantaneous peaks are substantially different from those predicted for isolated elements. These changes in dynamic loads must be considered for the design of structures with this configuration, which occasionally need some inclination either to deflect the flow or to optimize solar exposure or beam radiation. At 10^o of incidence (the radar aerial operating position), instantaneous peaks computed for two-dimensional forces reached up to five times the measured and computed mean value of normal loads, and twice the mean tangential loads. These are considerable increments if the structural design is based only on mean or static force coefficients.

CFD simulations with the *k-ω SST* turbulence model were able to capture the vortex shedding of the different elements with the same frequencies detected in experiments, although the turbulence energy spectrum in the panel wakes showed some discrepancies in intensity, which we attribute to the inherent limitations of RANS models.

The three-dimensional effects of an approximately square structure in a turbulent boundary layer flow increased the local forces on the different panels up to 95% above the values computed in 2-D simulations and wind tunnel tests.

All these considerations should be taken into account for the dynamic design loads.

A large number of factors influence these loads and deserve further investigation: angle of incidence, distance and distribution of elements and aspect ratios, to mention the most relevant. Further work includes a more exhaustive processing of data, further experimental measurements, and the analysis of the influence of parameters such as distance, geometry and distribution of structural elements, in order to find a configuration that minimizes the dynamic loads on panels.

Acknowledgements

This work was carried out under a cooperation agreement between INVAP S. A. and the National University of La Plata. The authors are grateful to the Argentine Air Force and the General Directorate for Military Procurements for their authorization to publish these results, and to our colleague Christopher Young for revising the paper draft.

References

Bacchi, F., Scarabino, A., Marañon Di Leo, J., Delnero, S., Boldes, U. and Colman, J. (2007), "Numerical and experimental determination of drag coefficients and strouhal numbers of a port crane section", *Proceedings of the 12th International Conference on Wind Engineering*, 727-734 Cairns, Australia, July 2007.

Bergh, H. and Tigdeman, H. (1965), "Theoretical and experimental results for the dynamic response of pressure measuring systems", National Aero- and Astronautical Research Institute Amsterdam. NLR-TR F.238.

Blackburn, H.M., Henderson, R.D. (1999), "A study of two-dimensional flow past an oscillating cylinder", *J. Fluid Mech*., **385**, 255-286.

Catalano, P. and Amato, M. (2003), "An evaluation of RANS turbulence modelling for aerodynamic applications", *Aerosp. Sci. Technol*., **7**(7), 493-509.

Chatterjee, D., Biswas, G. and Amiroudine, S. (2010), "Numerical simulation of flow past row of square cylinders for various separation ratios", *Comput. Fluids*, **39**(1), 49-59.

Fitzpatrick, J.A., Donaldson, I.S. and McKnight, W. (1988), "Strouhal numbers for flows in deep tube array models", *J. Fluid. Struct.*, **2**, 145-160.
Freitas, C.J. (1995), "Perspective: selected benchmarks for commercial CFD codes", *J. Fluid. Eng. - T ASME*, **117**, 208-218.
Hoerner, S.F. (1965), *Fluid-dynamic drag*, Hoerner Fluid Dynamics.
Holmes J.D. (2001), *Wind Loading of Structures*, ed. Taylor and Francis, London.
Kaimal, J.C. and Finnigan J.J. (1994), *Atmospheric Boundary Layer Flows*, Oxford University Press, Oxford.
Lam, K., Li, J.Y., Chan, K.T. and So, R.M.C. (2003), "Flow pattern and velocity field distribution of cross-flow around four cylinders in a square configuration at a low Reynolds number", *J. Fluids Struct*., **17**, 665-679.
Mannini, C., Weinman, K., Soda, A. and Schewe, G. (2009), "Three-dimensional numerical simulation of flow around a 1:5 rectangular cylinder", *Proceedings of the EACWE 5* Florence, Italy, 19th – 23rd July 2009.
Menter, F.R. (1994), "Two-equation eddy-viscosity turbulence models for engineering applications", *AIAA J.*, **32**(8), 1598-1605
Okajima, A. (1982), "Strouhal numbers of rectangular cylinders", *J. Fluid Mech.*, Cambridge University Press, **123**, 379-398.
Sachs, P. (1978), *Wind Forces in Engineering*, Pergamon Press.
Scarabino, A., Marañon di Leo, J., Delnero, J.S. and Bacchi, F. (2005), "Drag coefficients and strouhal number of a port crane boom girder section", *J. Wind Eng. Ind. Aerod*., **93**(6), 451-460.
So, R.M.C., Liu, Y., Chan, S.T. and Lam, K. (2001), "Numerical studies of a freely vibrating cylinder in a cross-flow", *J. Fluids Struct*., **15**, 845-866.
Sumner, D., Price, S.J. and Paidoussis, M.P. (2000), "Flow-pattern identification for two staggered circular cylinders in cross flow", *J. Fluid Mech*., **411**, 263-303.
Vikram, C.K., Krishne Gowda, Y.T. and Ravindra, H.V. (2012), "Influence of corner cutoffs on flow past square cylinder", *ICCIMIM* - 2012, July 2012.

AD